Three-dimensional transcranial microbubble imaging for guiding volumetric ultrasound-mediated blood-brain barrier opening

Ryan M. Jones[1], Lulu Deng[1], Kogee Leung[1], Dallan McMahon[1,2], Meaghan A. O'Reilly[1,2], and Kullervo Hynynen[1,2,3]

[1]*Physical Sciences Platform, Sunnybrook Research Institute, Toronto, Ontario, Canada*

[2]*Department of Medical Biophysics, University of Toronto, Toronto, Ontario, Canada*

[3]*Institute of Biomaterials and Biomedical Engineering, University of Toronto, Toronto, Ontario, Canada*

Supplementary Material

Array Module Optimization

Numerical simulations were carried out to optimize the transducer module layout prior to array construction. Five thousand distinct sparse configurations of 256 modules distributed over a 31.8 cm diameter hemispherical shell were pseudo-randomly generated, with the only constraint being that each array quadrant (3 top and 1 bottom, see **Figure 1A**) contained an equal number of modules (*i.e.*, $N = 64$). A cost function was used to rank the performance of each individual configuration [79]. For each candidate module configuration, transcranial simulations were carried out on transmit and receive at each of the three frequencies of interest (see **Table 1**) for five different source/target locations ([0,0,0], [±25,0,0], and [0,±25,0] mm). The largest of the peak sidelobe ratios obtained across different source/target locations was selected for each module configuration, as this worst-case scenario will be limiting in practice [79]. A small set of simulations found that using these five source locations was sufficient to predict the general performance of a given transducer array. The cost function was

calculated by averaging the worst-case peak sidelobe ratio values across each of the three frequencies tested, and across the results obtained from both transmit and receive simulations (intensity distributions in both cases). A histogram of the cost function distribution is plotted in **Figure S1**. The transducer module configuration with the lowest cost function was considered to be optimal and was selected for construction. From a fit of a normal distribution to the cost function histogram (**Figure S1**), it was estimated with 95% confidence that the chosen module layout would be within the best 0.1% of all possible configurations.

Array Transmit Characterization

Acoustic field measurements were performed in degassed/deionized water using a calibrated fiber-optic hydrophone (Precision Acoustics, Ltd., Dorset, UK). Each transmit frequency was characterized separately by driving the appropriate elements (100 μs pulse length, 1 Hz PRF) using a custom-built 256-channel driving system. The speed of sound in water was estimated by recording the water temperature [59] with a digital thermometer (Extech Instruments, Waltham, MA, USA) and was used, together with the measured element locations, to determine the element phasing required to focus the array to a given target within the field. Measurements were carried out at a total of 8 target locations spanning [0,60] mm along the X-axis and [-40,40] mm along the Z-axis by electronically steering the beam. At each target position, the temporal-peak negative acoustic field distributions (FOV = 2.4 $\lambda \times 2.4 \lambda$; pixel size = $\lambda/8 \times \lambda/8$, where λ denotes the acoustic wavelength in water) in the lateral (XY) and axial (XZ) planes were recorded by scanning the hydrophone using a three-axis positioning system (Superior Electric Motors, Inc., Bristol, CT, USA; Velmex, Inc., Bloomfield, NY, USA) for each of the array's three frequencies at a fixed driving system input voltage (*e.g.*, see **Figure S2** for 612 kHz data). The SPTP negative pressure as a function of the driving system input voltage was then measured for each operating frequency at the array's geometric focus. The hydrophone recordings were captured on a

digital oscilloscope (TDS 3014B; Tektronix, Inc., Richardson, TX, USA) and saved via General Purpose Interface Bus (GPIB) to a CPU for post-processing. Plots of the SPTP negative acoustic pressure and focal volume dimensions as a function of position within the field are given in **Figure S3** for all three operating frequencies. The array's effective beam steering range, defined here as the range over which the SPTP negative focal pressure is greater than or equal to 50% of the value obtained when targeting the geometric focus, was estimated for each operating frequency based on 1D Gaussian fits of the steering data (**Table S1**).

Supplementary Tables

Table S1. Gaussian fitting of transmit steering data. Summary of Gaussian fitting applied to transmit steering data at each of the array's operating frequencies. The fits correspond to a driving system input voltage of 90 V peak-to-peak for each operating frequency. Labels X and Z refer to fits to the lateral (X-axis) and axial (Z-axis) steering data, respectively. The errors quoted on the steering ranges are based on the uncertainty in the Gaussian fitting procedure. Coeff. = Coefficient.

Axis	Parameter	306 kHz	612 kHz	1224 kHz
	Amplitude (MPa)	1.87	1.49	1.21
	Mean (mm)	-	-	-
X	*Standard Deviation (mm)*	42.3	38.3	40.8
	Coeff. of Determination	0.99	0.99	0.99
	Steering Range (mm)	99 ± 3	90 ± 3	96 ± 3
	Amplitude (MPa)	1.80	1.46	1.13
	Mean (mm)	6.3	0.4	0.4
Z	*Standard Deviation (mm)*	41.1	36.3	26.8
	Coeff. of Determination	0.96	0.97	0.91
	Steering Range (mm)	97 ± 8	85 ± 5	63 ± 8

Supplementary Figures

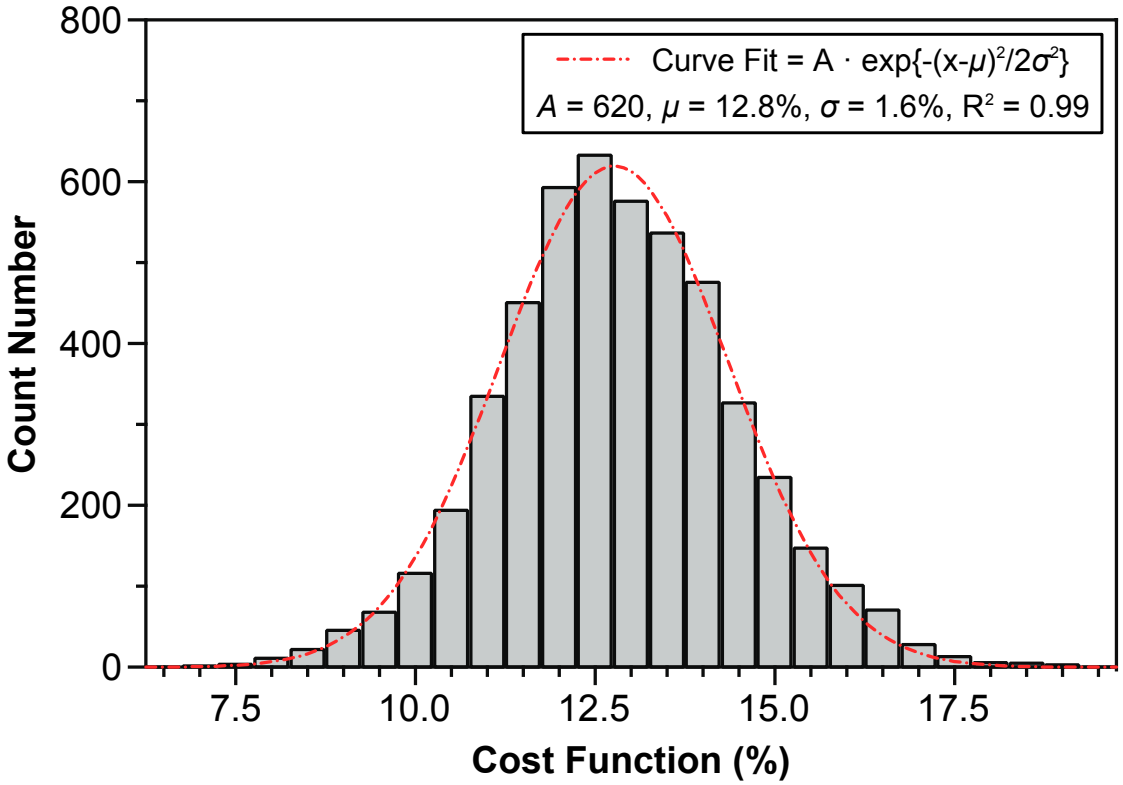

Figure S1. Cost function histogram of sparse module configurations. Cost function histogram of 5,000 sparse transducer module configurations (256 modules, 31.8 cm diameter hemispherical array). A normal distribution was fit to the data (red curve). A = amplitude; μ = mean; σ = standard deviation; R^2 = coefficient of determination.

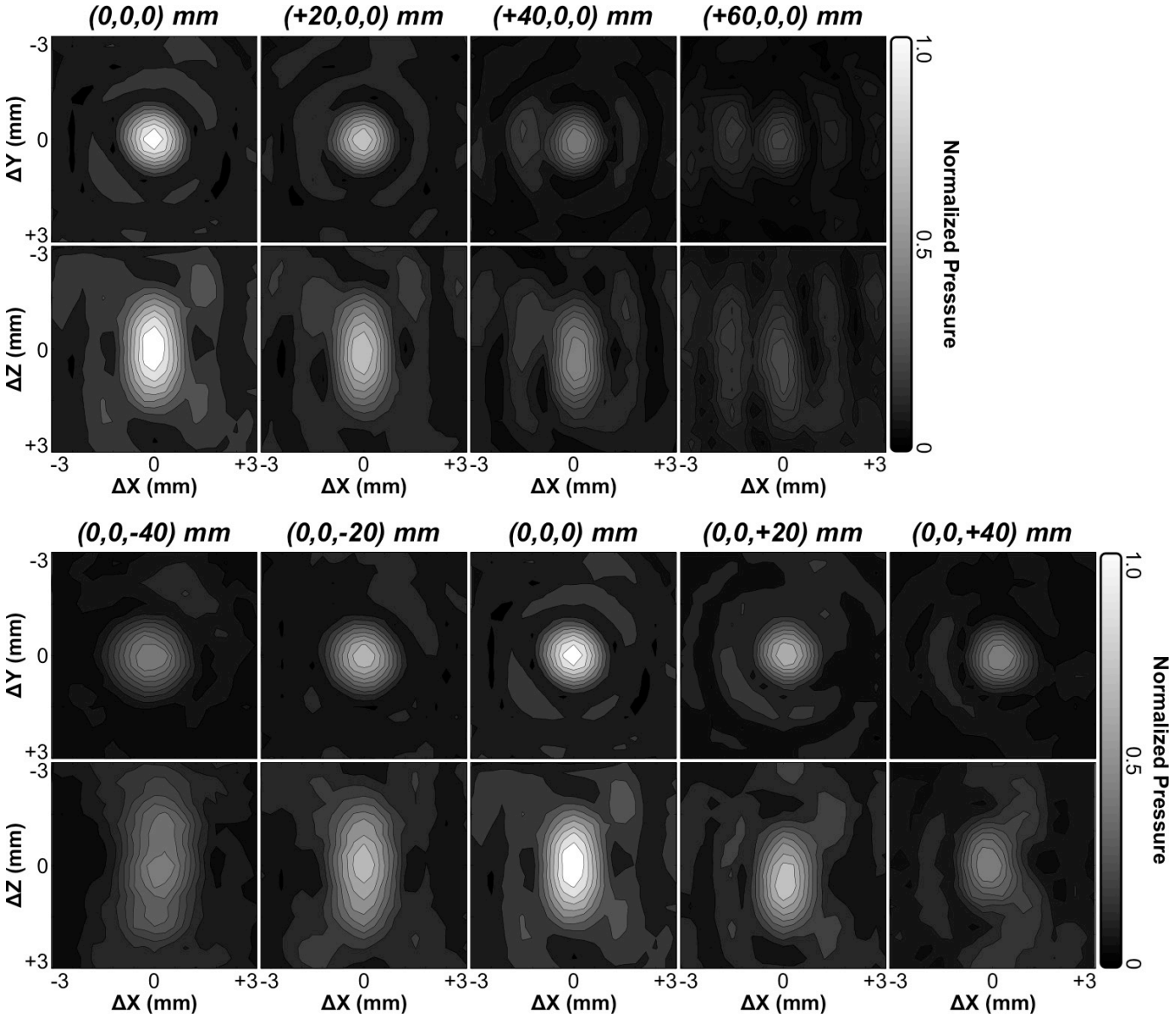

Figure S2. Transmit acoustic field distributions from clinical-scale prototype FUS brain system. Transmit lateral (XY plane) and axial (XZ plane) temporal-peak negative pressure distributions generated by the clinical prototype FUS brain system while steering the beam laterally (X-axis) and axially (Z-axis) at f_0 = 612 kHz. All plots are normalized to the SPTP negative pressure obtained when targeting the array's geometric focus. Linear contours are displayed at 10% intervals. Axis labels are given relative to the target location. Positive/negative values of Z indicate in/out of the hemispherical array (see **Figure 6D**).

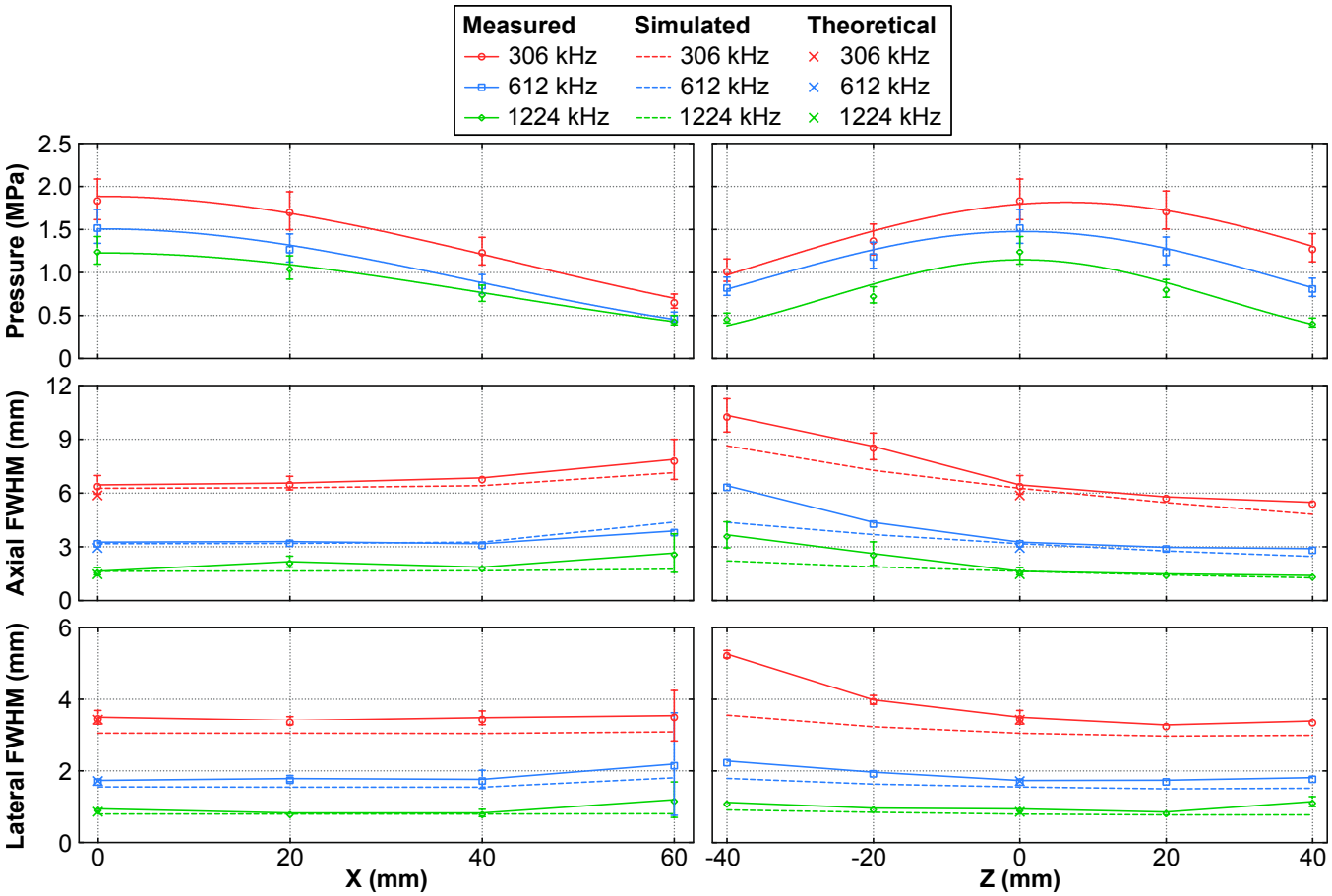

Figure S3. Transmit acoustic characterization of clinical-scale prototype FUS brain system. SPTP negative pressure and transmit focal size (pressure full-width at half-maximum (FWHM)) obtained in water as a function of target location for beam steering along lateral (X) and axial (Z) axes at each of the array's operational frequencies (f_0 = 306 kHz (red), 612 kHz (blue), 1224 kHz (green)). The SPTP negative pressure values (top row) correspond to a driving system input voltage of 90 V peak-to-peak for each operating frequency. The error bars on the acoustic pressure data are based on the uncertainty of the fiber-optic hydrophone system, and the error bars in the focal volume data represent one SD over repeated measurements (N = 3). 1D Gaussian fits were applied to the acoustic pressure steering data and added to the plots (see **Table S1** for fitting parameters). Simulated values (ray-acoustics model, see [61,77]) for the transmit focal size as a function of target location for each frequency are plotted as dashed lines, and the theoretical values at the natural focus of a single-element spherically curved radiator [80] are denoted by '×' symbols.

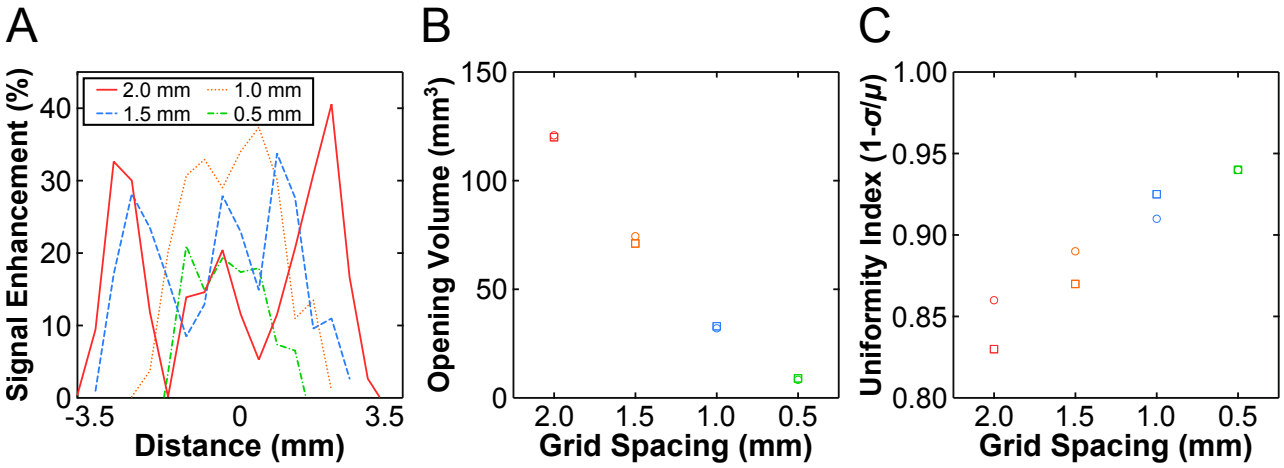

Figure S4. Variable point spacing during multi-point exposures: quantitative analysis. (A) Representative 1D line profiles of CE-T_1w MRI signal enhancement for different point-to-point spacings, based on the data presented in **Figure 4B** (f_0 = 612 kHz, 3 x 3 point grids, 75% target levels). **(B)** BBB opening volume and **(C)** uniformity index (μ = mean, σ = standard deviation) for each point-to-point spacing investigated, based on two independent datasets from an animal in the pilot group (circles/squares, circles correspond to axial plane presented in **Figure 4B**).

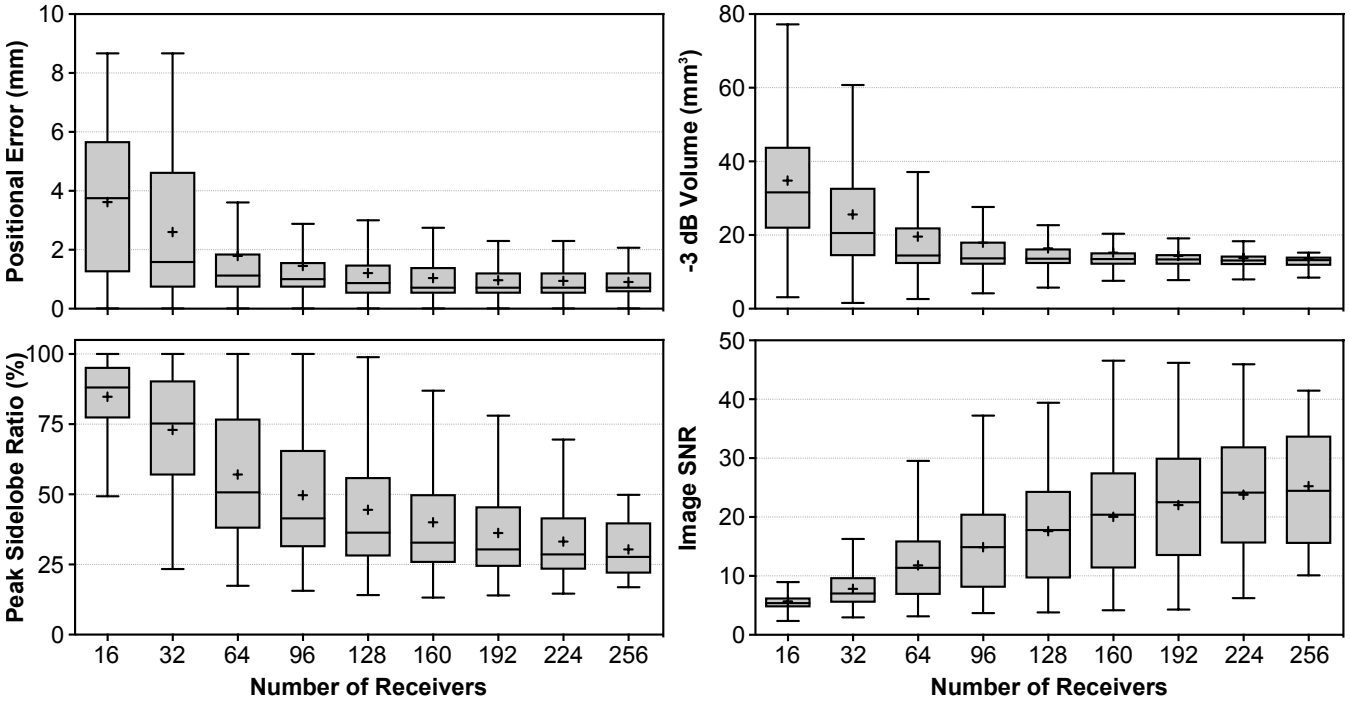

Figure S5. Image quality *in vivo* as a function of array sparsity. Tukey box and whisker plots of various image quality metrics as a function of receiver array sparsity using data from the treatment group (20 calibration sonications over 5 animals, 500 distinct element configurations per level of sparsity, $f_0/2$ = 306 kHz, FOV = 10 mm × 10 mm × 10 mm, voxel size = 0.5 mm × 0.5 mm × 0.5 mm). Positional error is defined as the distance between the location of SPTA source field intensity and the intended target. Image SNR is defined as the ratio of the SPTA source field intensity to the SD of the background signal (all voxels greater than a wavelength from the location of SPTA intensity [54]). The '+' symbol, horizontal line, and boxed region denote the mean, median, and interquartile range (IQR) values (*i.e.*, difference between the 25th and 75th percentiles), respectively. The lower (upper) error bar indicates the 25th percentile - 1.5×IQR (75th percentile + 1.5×IQR).